Dynamic Single-Pixel Imaging on an Extended Field of View without Warping the Patterns

Thomas Maitre[1], Elie Bretin[2], Romain Phan[1], Nicolas Ducros[1,3], and Michaël Sdika[1] *

[1] Univ Lyon, INSA-Lyon, Universite Claude Bernard Lyon 1, UJM-Saint Etienne, CNRS, Inserm, CREATIS UMR 5220, U1294, F-69621, LYON, France
[2] Univ Lyon, INSA de Lyon, CNRS UMR 5208, Institut Camille Jordan, F-69621 Villeurbanne, France
[3] Institut universitaire de France (IUF), France

Abstract. A single-pixel camera is a spatial-multiplexing device that reconstructs an image from a sequence of projections of the scene onto some patterns. This architecture is used, for example, to assist neurosurgery with hyperspectral imaging. However, capturing dynamic scenes is very challenging: as the different projections measure different frames of the scene, standard reconstruction approaches suffer from strong motion artifacts. This paper presents a general framework to reconstruct a moving scene with two main contributions. First, we extend the field of view of the camera beyond that defined by the spatial light modulator, which dramatically reduces the model mismatch. Second, we propose to build the dynamic system matrix without warping the patterns, effectively dismissing discretization errors. Numerical experiments show that both our contributions are necessary for an artifact-free reconstruction. The influence of a reduced measured set, robustness to noise and to motion errors were also evaluated.

Keywords: Single-pixel camera · Motion compensation · Image reconstruction.

1 Introduction

Single-pixel imaging (SPI) uses a single detector to measure the inner product between the scene and some user-defined light patterns [4]. This makes it possible to use detectors incompatible with matrix sensors, such as a spectrometer for fast hyperspectral imaging [1]. Such images can be used for a wide range of medical applications including cancers detection, cardiac disease, ischemic tissue, skin burn, kidney disease, etc [10]. In particular, it has been shown that hyperspectral imaging improves the identification of tumor margins in fluorescence-guided neurosurgery for the resection of gliomas [3].

The acquisition process leads to an inverse problem that can be solved with traditional optimization techniques [5, 6] or with machine learning approaches

* Corresponding author: michael.sdika@creatis.insa-lyon.fr

[13, 12, 14]. Because the measurements are acquired sequentially, SPI assumes the scene to remain static, otherwise resulting in important motion artifacts. Using a smaller measurement set helps the reconstruction by compromising between motion and compression artifacts. Even so, there are two fundamental steps to consider to achieve dynamic SPI completely free from motion artifacts: i) motion estimation and ii) reconstruction with a known motion.

In [16, 2], the motion is estimated on a low-resolution video reconstructed from few measurements. However, this only allows a rough estimation of the motion which may fail to capture complex motion models. Recently, a two-armed device combining a single-pixel camera and a conventional camera with high spatial resolution was proposed to address this problem [11].

There are two main ways to tackle the image reconstruction once the motion is known. The first aims at minimizing the optical-flow between subsequent frames along with the residual of the forward model, and eventually an appropriate *a priori* about the image [16, 19]. The second relies on motion compensation to build a new linear operator for the dynamic forward model [15, 17, 8]. In SPI, this has been used in very specific situations. For instance, [9] presents a discrete version of motion compensation that only works for rigid motions, [9, 11] limit their study to scenes where no new objects appear in the single-pixel camera (SPC) field of view (FOV) during the acquisition. Besides, in all these works, the problem is discretized by warping the light patterns to compensate the motion. However, warping the fine scale light pattern as in [11, 7] might lead to high discrepancy between the continuous and the discretized problem, even under small deformation. Previous works used TV regularization to attenuate these artifacts at the expense of losing image details. In practice, these assumptions are unrealistic in brain surgery where the object is pulsating in and out of the SPC's FOV and where good image quality is needed to help the surgeon identify tumorous regions. Applying the method proposed in [11] to such cases results in important artifacts.

In this work, we tackle these limitations with a new setting where we solve the dynamic problem on an extended FOV and build the dynamic forward model without warping the light patterns. We will show that only using both contributions allows an artifact-free reconstruction of the scene. The paper is organized as follows. Section 2 presents the necessary background on single-pixel imaging. Section 3 presents our two main contributions: a new method for dynamic single-pixel imaging on an extended FOV and a new discretization for the dynamic forward model that removes artifacts. Numerical experiments are presented and discussed in section 4.

2 Single-pixel imaging

2.1 Forward model

Static acquisition A single-pixel acquisition measures a sequence of inner products between the scene and some light patterns. When a static scene $f(\boldsymbol{x})$

is considered, the k^{th} measurement can be written as:

$$m_k = \int_X h_k(\boldsymbol{x}) f(\boldsymbol{x}) \, \mathrm{d}x, \tag{1}$$

where h_k is the k^{th} pattern and X is the SPC's FOV (which matches the support of h_k). This leads to the resolution of an inverse problem $\boldsymbol{m} = \boldsymbol{H}\boldsymbol{f}$ where $\boldsymbol{m} = [m_1, \dots, m_K]^\top \in \mathbb{R}^K$ is the measurement vector, $\boldsymbol{f} \in \mathbb{R}^N$ is the discrete image of the scene with N pixels, and $\boldsymbol{H} \in \mathbb{R}^{K \times N}$ is the measurement matrix containing all the patterns.

Dynamic acquisition For dynamic scenes $f(t, \boldsymbol{x})$, the k^{th} measurement is modeled in a similar fashion by:

$$m_k = \int_X h_k(\boldsymbol{x}) f_k(\boldsymbol{x}) \, \mathrm{d}x, \tag{2}$$

where $f_k = f(t_k, \cdot)$ represents the k^{th} frame of the scene. As K frames cannot be estimated from only K scalar measurements, [11] assumes that the scene can be motion compensated, i.e.,

$$f_k \circ v_k = f_{\text{ref}}, \tag{3}$$

where v_k is the deformation occurring between times t_k and t_{ref} and f_{ref} is the reference motion-compensated image. Then, assuming that f_{ref} is supported in X, the forward problem can be written $\boldsymbol{m} = \boldsymbol{H}_{\text{dyn}} \boldsymbol{f}_{\text{ref}}$ where $\boldsymbol{H}_{\text{dyn}} \in \mathbb{R}^{K \times N}$ is the dynamic matrix and $\boldsymbol{f}_{\text{ref}} \in \mathbb{R}^N$ is the discrete reference image.

2.2 Image reconstruction

In the presence of noise and/or when considering an accelerated acquisition with a reduced number of measurements (i.e., $K < N$), the image can be reconstructed by optimization of a hand-crafted objective

$$\min_{\boldsymbol{f}} \frac{1}{2} \|\boldsymbol{A}\boldsymbol{f} - \boldsymbol{m}\|_2^2 + \eta \mathcal{R}(\boldsymbol{f}), \tag{4}$$

where $\boldsymbol{A}$ is the system matrix (i.e., $\boldsymbol{H}$ for static acquisitions and $\boldsymbol{H}_{\text{dyn}}$ for dynamic acquisitions), η is the regularization parameter and $\mathcal{R}$ is a regularization functional. The system matrix $\boldsymbol{H}$ is often chosen in bases such as Hadamard or Fourier and is therefore often well-conditioned. However, the dynamic matrix $\boldsymbol{H}_{\text{dyn}}$ turns out to be ill-conditioned and, therefore, the dynamic reconstruction problem requires regularization even in the case $K = N$.

3 Method

3.1 Dynamic forward model with extended FOV

The method introduced in [11] assumes that either the reference image is null outside the SPC's FOV or that the motion does not modify the scene on the

FOV's borders. Neither of these assumptions are realistic for practical applications such as fluorescence guided neurosurgery: the brain is a continuous object also defined outside the SPC's FOV and subject to a motion (mainly due to cardiac pulsations). This motion implies that information goes in and out of the SPC's FOV and induce a bias in the model.

To cope with this problem, we start by plugging (3) into (2):

$$\begin{aligned} m_k &= \int_X h_k(\boldsymbol{x}) f_{\text{ref}}(v_k^{-1}(\boldsymbol{x}))\,\mathrm{d}\boldsymbol{x} = \int_{Z_k} h_k(v_k(\boldsymbol{z})) f_{\text{ref}}(\boldsymbol{z})\,|J_k(\boldsymbol{z})|\,\mathrm{d}\boldsymbol{z} \\ &= \int_{Z_k} h_k^{\text{dyn}}(\boldsymbol{z}) f_{\text{ref}}(\boldsymbol{z})\,\mathrm{d}\boldsymbol{z}, \end{aligned}$$

where $h_k^{\text{dyn}}(\boldsymbol{z}) := |J_k(\boldsymbol{z})|\, h_k(v_k(\boldsymbol{z}))$ is the dynamic pattern, J_k is the Jacobian of v_k, and $Z_k := v_k^{-1}(X)$ is the support of the dynamic pattern h_k^{dyn}. Then, contrary to [11] that integrates over X, we introduce an extended reconstruction domain X_{ext} that includes all the Z_k and obtain:

$$m_k = \int_{X_{\text{ext}}} h_k^{\text{dyn}}(\boldsymbol{x}) f_{\text{ref}}(\boldsymbol{x})\,\mathrm{d}\boldsymbol{x} \neq \int_X h_k^{\text{dyn}}(\boldsymbol{x}) f_{\text{ref}}(\boldsymbol{x})\,\mathrm{d}\boldsymbol{x}. \tag{5}$$

Discretization of (5) on a regular grid of L pixels that covers X_{ext} leads to the dynamic forward model $\boldsymbol{m} = \boldsymbol{H}_{\text{dyn}}^v \boldsymbol{f}_{\text{ref}}$, where $\boldsymbol{H}_{\text{dyn}}^v \in \mathbb{R}^{K\times L}$ is the dynamic system matrix on the extended FOV, $\boldsymbol{f}_{\text{ref}} \in \mathbb{R}^L$ and $\boldsymbol{m} \in \mathbb{R}^K$. Note that Equation (5) can be seen as an acquisition in a virtual space where the scene is static and the patterns are warped (Fig. 2e), in opposition to the physical acquisition where the scene is warped and the patterns are static (Fig. 2a).

3.2 Dynamic system matrix without warping the patterns

Although equations (2) and (5) are equivalent, warping of the light patterns in the latter in a discrete setting may raise numerical issues. For example, a compression warp of highly oscillating binary patterns will result in smooth blurry patterns, leading to a strong discrepancy between the continuous and the discrete models. To avoid warping the patterns, we discretize (2) in the physical space. We search the reference frame on the extended FOV in a certain basis of functions (e.g. B-splines):

$$f_{\text{ref}}(\boldsymbol{x}) = \sum_{j\in I_{\text{ext}}} f_{\text{ref}}^j \beta(\boldsymbol{x} - \boldsymbol{x}_j), \tag{6}$$

where the f_{ref}^j's are the discrete reference frame coefficients, β is the basis function and I_{ext} are the indexes necessary to cover X_{ext}. Then, the k^{th} acquisition from (2) can be written as:

$$m_k = \int_X h_k(\boldsymbol{x}) f_{\text{ref}}(u_k(\boldsymbol{x}))\,\mathrm{d}x = \sum_{j\in I_{\text{ext}}} f_{\text{ref}}^j \int_X h_k(\boldsymbol{x}) \beta(u_k(\boldsymbol{x}) - \boldsymbol{x}_j)\,\mathrm{d}x. \tag{7}$$

where $u_k = v_k^{-1}$. After discretizing the integral, this equation becomes:

$$m_k = \sum_{j \in I_{\text{ext}}} f_{\text{ref}}^j \sum_{i \in I} h_k(\boldsymbol{x_i}) u_{i,j}^k, \tag{8}$$

where $u_{i,j}^k = \beta(u_k(\boldsymbol{x}_i) - \boldsymbol{x}_j)$ and I is the portion of I_{ext} that covers X. As (8) is linear in f_{ref}, it can be written as $\boldsymbol{m} = \boldsymbol{H}_{\text{dyn}}^p \boldsymbol{f}_{\text{ref}}$, where $\boldsymbol{H}_{\text{dyn}}^p$ is the dynamic system matrix in the physical space. Note that $u_{i,j}^k$ can be nonzero for j outside I, which justifies the need of an extended FOV for the reconstruction. In practice, the support of the B-splines being quite small, the majority of $(u_{i,j}^k)_{i,j}$ coefficients are null which makes the computation of (8) efficient.

4 Results

Experimental settings For this study, we consider a 90×90 image of a brain surface subject to the deformation:

$$u_k(\boldsymbol{x}) = \boldsymbol{c} + \begin{pmatrix} s(t_k) & 0 \\ 0 & s(t_k)^{-1} \end{pmatrix} (\boldsymbol{x} - \boldsymbol{c}), \tag{9}$$

where $s(t) = 1 + a\sin(\frac{2\pi t}{T})$, $a = 0.2$ is the motion amplitude, $T = 1000$ ms the motion period and $\boldsymbol{c}$ is the coordinate of the center of the image. We consider the motion known at each frame. The SPC's FOV covers an area of 64×64 pixels in the center of the image. We acquire 64^2 measurements according to the forward model (2) with Hadamard patterns during 2 periods of the motion. We consider the three regularizers L^2 ($\mathcal{R} = \frac{1}{2}\|\cdot\|_2^2$), H^1 ($\mathcal{R} = \frac{1}{2}\|\nabla\cdot\|_2^2$) and H^2 ($\mathcal{R} = \frac{1}{2}\|\nabla^2\cdot\|_2^2$), for which the variational problem have a closed-form solution. We compare it to the TV ($\mathcal{R} = \|\nabla\cdot\|_1$) regularizer employed in [11]. As the objective in this work is to validate the system matrix itself, it is important not to use learning-based regularizers that might possibly compensate potential artifacts.

First, we validate our method by reconstructing the reference (8100 pixels) from noiseless measurements with all 4096 measurements. Then, we conduct experiments to certify the robustness of the model when the measurement vector is incomplete, when it is corrupted by noise or when the motion is estimated.

Visualizing the discretization biases The map in Fig. 1a is the percentage of measurements that contributes to the reconstruction of each pixel. During an acquisition, the measurement vector $\boldsymbol{m}$ incorporates information from all non-black pixels. If $\boldsymbol{H}_{\text{dyn}}$ is built using pixels in X only (instead of X_{ext}), the reconstruction sends the information from the pixels outside X to pixels inside X, creating some artifacts. The three right images presented on the right of Fig. 1 are the models' biases, measured as $\log|\boldsymbol{H}_{\text{dyn}}\boldsymbol{f}_{\text{ref}} - \boldsymbol{m}|$. One can observe an important bias when discretizing the patterns in the virtual space (Fig. 1b). When discretizing in the physical space but reconstructing in X only (Fig. 1c), the bias is even more important. In contrast, the model resulting from the combination of the reconstruction in X_{ext} with our physical discretization leads to a consistent representation of the reality, with little to no bias in the forward model (Fig. 1d).

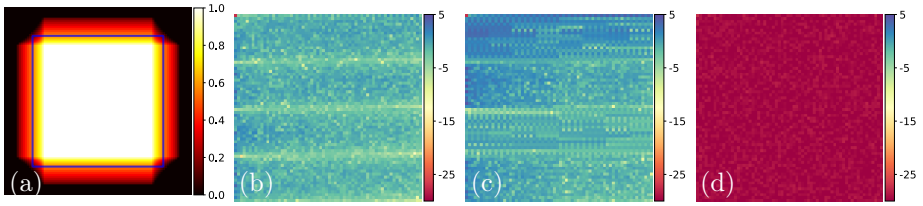

Fig. 1. (a) Contribution map of the measurements with the SPC's FOV in blue. Residual map in logarithmic scale from: (b) the virtual discretization from (5) in X_{ext}, (c) the physical discretization (8) in X, (d) the physical discretization (8) in X_{ext}.

Ablation study For the ground truth image displayed in Fig. 2i, we showcase the effect of each of our two contributions in the top right of Fig. 2 with L^2 regularization on the first line and H^1 in the second line. The first column reconstructs the image on an extended FOV as in Section 3.1 with just enough regularization ($\eta = 10^{-10}$) to cope with the ill-posed nature of the problem. One can see the artifacts originating from the virtual discretization of (5). The second column uses our physical discretization (8) on X only. As a consequence of the important bias observed in Fig. 1c, we had to choose an important regularization parameter ($\eta = 10^3$) to perform the reconstruction. The last column demonstrates the effectiveness of the combination of both our contributions with almost no regularization ($\eta = 10^{-10}$). If the conclusions are similar for both regularization, one can clearly see that H^1 leads to a far better reconstruction, almost indistinguishable from the ground truth within the SPC's FOV.

Comparison to state of the art The results from the state of the art are presented in the bottom right of Fig. 2. The static forward model (Eq. (4) with $\boldsymbol{H}$) results in important artifacts, as shown in Fig. 2j. The dynamic model presented in [11] (Eq. (4) using $\boldsymbol{H}_{\text{dyn}}$ and $\eta = 10^2$ for TV regularization) reconstructs an oversmoothed image with visible Gibbs artifacts in the corners that increase over the iterations, reduced by adopting a truncation strategy (Fig. 2k). Using a L^2 *a priori* in Fig. 2l improves this aspect, but important regularization ($\eta = 10^3$) is still mandatory even with noiseless measurements, demonstrating that the problem is not correctly modeled. In any cases, it is clear that our proposed method (Fig. 2h) outperforms any of the state of the art reconstructions.

Using a reduced set of measurements An advantage of the SPC is its ease of reconstruction from few measurements. We evaluate the robustness of the proposed approach on reduced sets of measurements using the peak signal-to-noise ratio (PSNR) of the reconstruction within the SPC's FOV. Results with structural similarity lead to similar conclusions (see supplementary material). In Fig. 3a, the PSNR was computed for a motion known exactly. Except for the method from the state of the art that heavily relies on regularization ($\eta = 10^3$), we set η to 10^{-10} because having more *a priori* for noiseless measurements was not particularly helpful. Overall, we remark that our contributions outperforms the

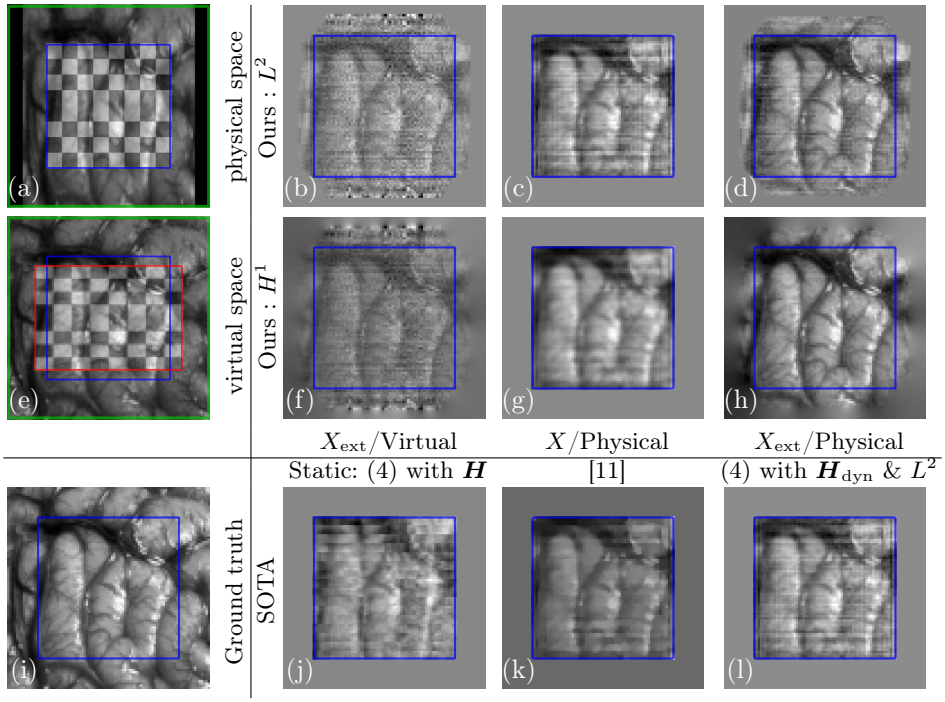

Fig. 2. Top left: The extended FOV in the physical and virtual spaces. X, X_{ext} and Z_k are respectively represented in blue, green and red. **Bottom left:** The ground truth. **Top right:** Reconstruction with our method: in line, the regularization L^2 or H^1. In column, with X or X_{ext} in the physical or virtual space. **Bottom right:** Reconstructions from the state of the art. From left to right: Static reconstruction from (4) with $\boldsymbol{H}$, Reconstruction from [11], Reconstruction L^2 from (4) with $\boldsymbol{H}_{\text{dyn}}$.

state of the art method. For a fixed number of measurement, H^1 and H^2 regularizers returns the highest scores. We observe a steady decrease of PSNRs as we reconstruct from fewer measurements. For L^2, the two metrics are considerably lower than for H^1 and H^2 and also gradually decreasing.

Robustness to noise We consider measurements corrupted by a Poisson noise $\boldsymbol{m} \sim \frac{1}{\alpha}\mathcal{P}(\alpha \boldsymbol{H}^p_{\text{dyn}} \boldsymbol{f}_{\text{ref}})$, with α a parameter representative of the number of photons that actually hits the detector. For each noise level, we empirically select a suitable regularization parameter on a single sample so as to maximize the reconstructions' PSNR. We then conduct the simulations on 20 different samples to obtain results independent of the distribution for a fixed α. We present results with a perfectly known motion in Fig. 3c. We observe a slight gradual decrease of both scores as the noise level increase, demonstrating the robustness of our method to noise. The best results are obtained with H^2 regularization, closely followed by H^1. Even though L^2 performances are lower, they are still considerably better than those obtained using the state of the art approach.

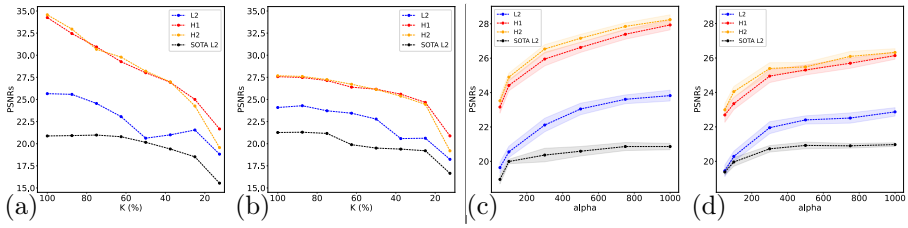

Fig. 3. Robustness of the proposed method. (a-b) PSNRs as a function of the number of measurement with known (Fig. 3a) and estimated motion (Fig. 3b). (c-d) PSNRs as a function of the noise level with known (Fig. 3c) and estimated motion (Fig. 3d). The shaded area represent the 95% confidence interval around the mean.

Robustness to motion errors We estimated the motion in X from a grayscale video of the scene at the SPC's FOV resolution with a motion estimation method [18]. We used constant extrapolation to get a rough idea of the motion in X_{ext}. After adjusting the regularization parameters, we confronted our method to reduced measurement sets and to Poisson noise in Fig. 3b and Fig. 3d. Despite a slight inevitable decrease in scores, we observed the same trends as in Fig. 3a and Fig. 3c, where H^1 and H^2 are the best regularizers. Both Fig. 3b and Fig. 3d show that even with a rough idea of the motion, our proposed method ensures reliable reconstructions of dynamic scenes. In practice, using a high-spatial resolution camera to estimate the motion of the scene [11] directly in the extended FOV X_{ext} will enable achieving results closer to Fig. 3a and Fig. 3c.

5 Conclusion

We proposed a new framework to reconstruct dynamic scenes for SPI including two important contributions. In particular, we demonstrated with numerical experiments that reconstructing on an extended FOV and using a physical discretization of the dynamic forward operator was the only way to correctly model the acquisition. This work will be implemented in an open-access python library[4]. Now that the problem modelisation is consistent with the reality and that reconstruction with classical regularizers is artifact-free, a promising lead for future works would be to consider deep learning-based regularizers (e.g. with diffusion models). Another interesting study would be to validate the feasibility of the method on hyperspectral data.

Acknowledgments. This study was funded by the French National Research Agency (ANR), under Grant ANR-22-CE19-0030-01 (ULHYB Project) and performed within the framework of the LABEX PRIMES (ANR-11-LABX-0063) of Université de Lyon, within the program "Investissements d'Avenir" operated by the French National Research Agency (ANR).

[4] https://github.com/openspyrit/spyrit

Disclosure of Interests. The authors have no competing interests to declare that are relevant to the content of this article.

References

1. Beneti Martins, G., Mahieu-Williame, L., Baudier, T., Ducros, N.: OpenSpyrit: an ecosystem for open single-pixel hyperspectral imaging. Optics Express **31**(10), 15599 (May 2023). https://doi.org/10.1364/OE.483937, https://opg.optica.org/abstract.cfm?URI=oe-31-10-15599
2. Bi, S., Zeng, X., Tang, X., Qin, S., Lai, K.W.C.: Compressive video recovery using block match multi-frame motion estimation based on single pixel cameras. Sensors **16**(3), 318 (2016)
3. Bravo, J.J., Olson, J.D., Davis, S.C., Roberts, D.W., Paulsen, K.D., Kanick, S.C.: Hyperspectral data processing improves ppix contrast during fluorescence guided surgery of human brain tumors. Scientific reports **7**(1), 9455 (2017)
4. Duarte, M.F., Davenport, M.A., Takhar, D., Laska, J.N., Sun, T., Kelly, K.F., Baraniuk, R.G.: Single-pixel imaging via compressive sampling. IEEE signal processing magazine **25**(2), 83–91 (2008)
5. Edgar, M.P., Gibson, G.M., Padgett, M.J.: Principles and prospects for single-pixel imaging. Nature photonics **13**(1), 13–20 (2019)
6. Gibson, G.M., Johnson, S.D., Padgett, M.J.: Single-pixel imaging 12 years on: a review. Optics express **28**(19), 28190–28208 (2020)
7. Hahn, B.N.: Efficient algorithms for linear dynamic inverse problems with known motion. Inverse Problems **30**(3), 035008 (2014)
8. Jiao, J., Bousse, A., Thielemans, K., Burgos, N., Weston, P.S., Schott, J.M., Atkinson, D., Arridge, S.R., Hutton, B.F., Markiewicz, P., et al.: Direct parametric reconstruction with joint motion estimation/correction for dynamic brain PET data. IEEE transactions on medical imaging **36**(1), 203–213 (2016)
9. Jiao, S., Sun, M., Gao, Y., Lei, T., Xie, Z., Yuan, X.: Motion estimation and quality enhancement for a single image in dynamic single-pixel imaging. Optics Express **27**(9), 12841 (Apr 2019). https://doi.org/10.1364/OE.27.012841, https://opg.optica.org/abstract.cfm?URI=oe-27-9-12841
10. Lu, G., Fei, B.: Medical hyperspectral imaging: a review. Journal of biomedical optics **19**(1), 010901–010901 (2014)
11. Maitre, T., Bretin, E., Mahieu-Williame, L., Sdika, M., Ducros, N.: Hybrid single-pixel camera for dynamic hyperspectral imaging. In: 2024 IEEE 21st International Symposium on Biomedical Imaging (ISBI). IEEE (2024)
12. Mur, A.L., Leclerc, P., Peyrin, F., Ducros, N.: Single-pixel image reconstruction from experimental data using neural networks. Optics Express **29**(11), 17097–17110 (2021)
13. Mur, A.L., Peyrin, F., Ducros, N.: Recurrent neural networks for compressive video reconstruction. In: 2020 IEEE 17th International Symposium on Biomedical Imaging (ISBI). pp. 1651–1654. IEEE (2020)
14. Mur, A.L., Peyrin, F., Ducros, N.: Deep expectation-maximization for single-pixel image reconstruction with signal-dependent noise. IEEE Transactions on Computational Imaging **8**, 759–769 (2022)
15. Rit, S., Sarrut, D., Desbat, L.: Comparison of analytic and algebraic methods for motion-compensated cone-beam CT reconstruction of the thorax. IEEE transactions on medical imaging **28**(10), 1513–1525 (2009)

16. Sankaranarayanan, A.C., Xu, L., Studer, C., Li, Y., Kelly, K.F., Baraniuk, R.G.: Video compressive sensing for spatial multiplexing cameras using motion-flow models. SIAM Journal on Imaging Sciences **8**(3), 1489–1518 (2015)
17. Scannell, C.M., Villa, A.D., Lee, J., Breeuwer, M., Chiribiri, A.: Robust non-rigid motion compensation of free-breathing myocardial perfusion MRI data. IEEE transactions on medical imaging **38**(8), 1812–1820 (2019)
18. Sdika, M., Alston, L., Rousseau, D., Guyotat, J., Mahieu-Williame, L., Montcel, B.: Repetitive motion compensation for real time intraoperative video processing. Medical Image Analysis **53**, 1–10 (2019)
19. Xu, Y., Lu, L., Saragadam, V., Kelly, K.F.: A compressive hyperspectral video imaging system using a single-pixel detector. Nature Communications **15**(1), 1456 (2024)